Available online at www.sciencedirect.com
SCIENCE DIRECT®
Journal of Magnetic Resonance 175 (2005) 309–316
JMR Journal of Magnetic Resonance
www.elsevier.com/locate/jmr

Magnetic material in head, thorax, and abdomen of *Solenopsis substituta* ants: A ferromagnetic resonance study

L.G. Abraçado [a], D.M.S. Esquivel [a], O.C. Alves [b], E. Wajnberg [a,*]

[a] *Departamento de Matéria Condensada e Espectroscopia, Centro Brasileiro de pesquisas Físicas, Rio de Janeiro, R. Xavier Sigaud 150, 22290-180 Rio de Janeiro, Brazil*
[b] *Departamento de Físico-Química da Universidade Federal Fluminense, Niterói 24020-150, Brazil*

Received 16 February 2005; revised 5 May 2005
Available online 6 June 2005

Abstract

Ferromagnetic resonance temperature dependence is used to study the magnetic material in smashed head, thorax, and abdomen of *Solenopsis substituta* ants. These three body parts present the five lines previously observed in other social insects. The magnetic material content is slightly higher in heads with antennae than in abdomen with petiole. Isolated nanoparticle diameters were estimated as 12.5 ± 0.1 and 11.0 ± 0.2 nm in abdomen with petiole and head with antennae, respectively. The presence of linear chains of these particles or large ellipsoidal particles are suggested. A bulk-like magnetite particle was observed in the thorax. The Curie–Weiss, the structural–electronic and ordering transition temperatures were obtained in good agreement with those proposed for magnetite nanoparticles.

Keywords: Fire ants; FMR; Magnetic nanoparticles; Magnetic volume; Temperature transitions

1. Introduction

Animals use several orientation mechanisms, among them those based on the geomagnetic field as a cue. Magnetoreception is a sophisticated orientation mechanism, involving a magnetoreceptor, connected to the nervous system with signal amplification. Under the physical point of view, the ferromagnetic hypothesis [1,2] is the most accepted one. It is based on the presence of ferromagnetic particles as the magnetoreceptor and supported by the detection of magnetite particles in a wide variety of animals, from insects [3,4] to humans [5,6]. Recently, a model was proposed considering the interactions among closely spaced clusters of superparamagnetic magnetite present in the upper-beak of homing pigeons. These interactions, induced by a variable magnetic field, result in a stress on the surrounding cellular structures [7,8].

It has been demonstrated that a few insects orient with the geomagnetic field [1] and ants respond to magnetic field changes. A magnetic compass response has been shown for Formica *rufa* [9] and *Oecophylla smaragdina* foraging [10]. *Atta colombica* ants respond to magnetic reversal in the absence of sunlight cues [11]. The magnetic effects on the time for trail formation by *Solenopsis invicta* ants are not clear [12,13], however, a role for magnetic cues in determining direction during ant orientation can be suggested.

Solenopsis ants are easily found and are widely spread in Brazil. These features turn this specie an interesting model for magnetic orientation studies, as it allow comparative analysis among nests in different location and geophysical conditions.

SQUID magnetometry and ferromagnetic resonance (FMR) are useful techniques to verify the ferromagnetic

* Corresponding author. Fax: +55 21 2141 7540
E-mail address: elianew@cbpf.br (E. Wajnberg).

1090-7807/$ - see front matter © 2005 Elsevier Inc. All rights reserved.
doi:10.1016/j.jmr.2005.05.006

hypothesis by localizing and characterizing the magnetoreceptor with no need for purification. FMR has the advantage of detecting only paramagnetic and ferro(i)magnetic substances and their interactions with the neighborhood. However, only relatively large amounts of magnetic material can be detected. The signal dependence on nanoparticles size, shape, and orientation, due to the anisotropy and demagnetization field contributions is an important feature [14–16].

There are few studies on magnetic materials in different body parts of social insects. It is well accepted that magnetite particles in *Apis mellifera* bee abdomen are involved in magnetoreception [17–19]. These studies were fostered by behavior assessment of trained honeybees that had magnets placed in their abdomens [20]. Susceptibility and magnetization measurements have shown typical paramagnetism with small magnetic remanence down to 4.2 K in the abdomen of adult worker honeybees while thorax and head showed an apparently diamagnetic behavior [21].

Hysteresis at 300 K of *Pachycondyla marginata* ants oriented body parts showed that the most relevant contribution to the ant saturation magnetization comes from the antennae. This sensory organ appears as a good candidate to a magnetoreceptor [22], once their migration was observed to be significantly oriented 13° relative to the magnetic North–South axis [23].

Previous FMR studies of crushed whole *Solenopsis* sp. ants [4], intact *Neocapritermes opacus* termites [24] and abdomens of migratory ant *P. marginata* and honeybee *A. mellifera* [14,15] showed the presence of different magnetic materials. Induced Remanent Magnetization (IRM) of *Nasutitermes exitiosus* [25] and FMR of *N. opacus* [24] indicated more magnetic material present in the thorax plus abdomen than in the termite head.

Magnetic material identification, localization, and characterization in ant body parts are necessary to the understanding the magnetoreceptor function. This paper reports the *S. substituta* ants abdomen with petiole-ABD, head with antennae-HEAD and thorax with feet-THOR FMR spectra dependence on temperature.

2. Materials and methods

Solenopsis substituta workers were collected in Fernando de Noronha, Pernambuco, Brazil, carefully washed with 70% (v/v) ethanol, until no particles were observed under a optical microscope (Micronal, AO-101 model), and preserved in 70% (v/v) ethanol. Just before measuring, they were dried on a filter paper for about 3 h at room temperature and separated into three parts: ABD (290 units), HEAD (250 units), and THOR (250 units), dried at 50 °C for 1 h, smashed, and transferred to quartz ferromagnetic resonance (FMR) tubes.

Measurements were performed with a commercial X-band EPR spectrometer (Bruker ESP300E) operating at a microwave power of 4 mW with a 100 kHz modulation frequency and a ~2 Oe modulation field amplitude, from 3 K to room temperature (RT). Spectra double integration was obtained using WINEPR software (Bruker).

Body part spectra were fitted using Origin 6.0 (Microcal) with two or three components: the high field (HF and HF′) and the low field (LF). Gaussian and Lorentzian derivative-shaped lines were used to obtain the temperature dependence of the resonance linewidth (ΔH_{pp}), resonance field (H_R), and absorption area (A) of HEAD and ABD spectra. Lorentzian (HF) and Dysonian (LF) shaped lines were used for THOR spectra. The Dysonian line is the combination of absorption and dispersion Lorentzian curves, expressed by Eq. (1) as a function of R_{ad}, the absorbed and dispersed microwave energy rate.

$$\begin{aligned} {}^{D}Y'(H) = B\{\{[1-(2(H-H_R)/\Delta H_{pp})^2] \\ \times R_{ad} - 4(H-H_R)/\Delta H_{pp}\} \\ /[1+(2(H-H_R)/\Delta H_{pp})^2]^2\}, \end{aligned} \quad (1)$$

where H_R and ΔH_{pp} are the parameters of the Lorentzian absorption derivative.

3. Results

The *S. substituta* ant parts spectra dependence on temperature is shown in Fig. 1. Each spectrum is composed of at least five components. An asymmetric line at $g = 4.3$ which intensity increases as temperature decreases, is characteristic of magnetically isolated high spin $S = 5/2$ Fe^{3+} ions in low-symmetry environment [26]. The narrow line at $g = 2$ is related to free radicals resulting from biological processes [27]. In the ABD and HEAD spectra, a broad line (~1000 Oe linewidth) at $g \sim 2$, called HF, is easily observed. Superimposed on this line, HF′ (about 300 Oe width) is resolved only at low temperatures. At RT a low field broad component (LF) is observed as a shoulder around $g = 4.3$ in the ABD and HEAD spectra, while in the THOR spectra, it is at $g = 18$ (position field where the amplitude is null) with a different lineshape predominant in the whole temperature range. In Fig. 1, examples of fitted curves (FIT) with the three components described above are shown, at 50 K, RT, and 4 K for the ABD, HEAD, and THOR, respectively.

The area under the absorption curve, S, is proportional to the number of FMR resonant spins. The LF component is dominant in the THOR spectra and it spreads out to negative field values that turns difficult S calculation of these spectra. However, based on the proportionality $S \propto I_{pp} \times \Delta H_{pp}^2$, a lower limit, 1.1×10^9 a.u., is

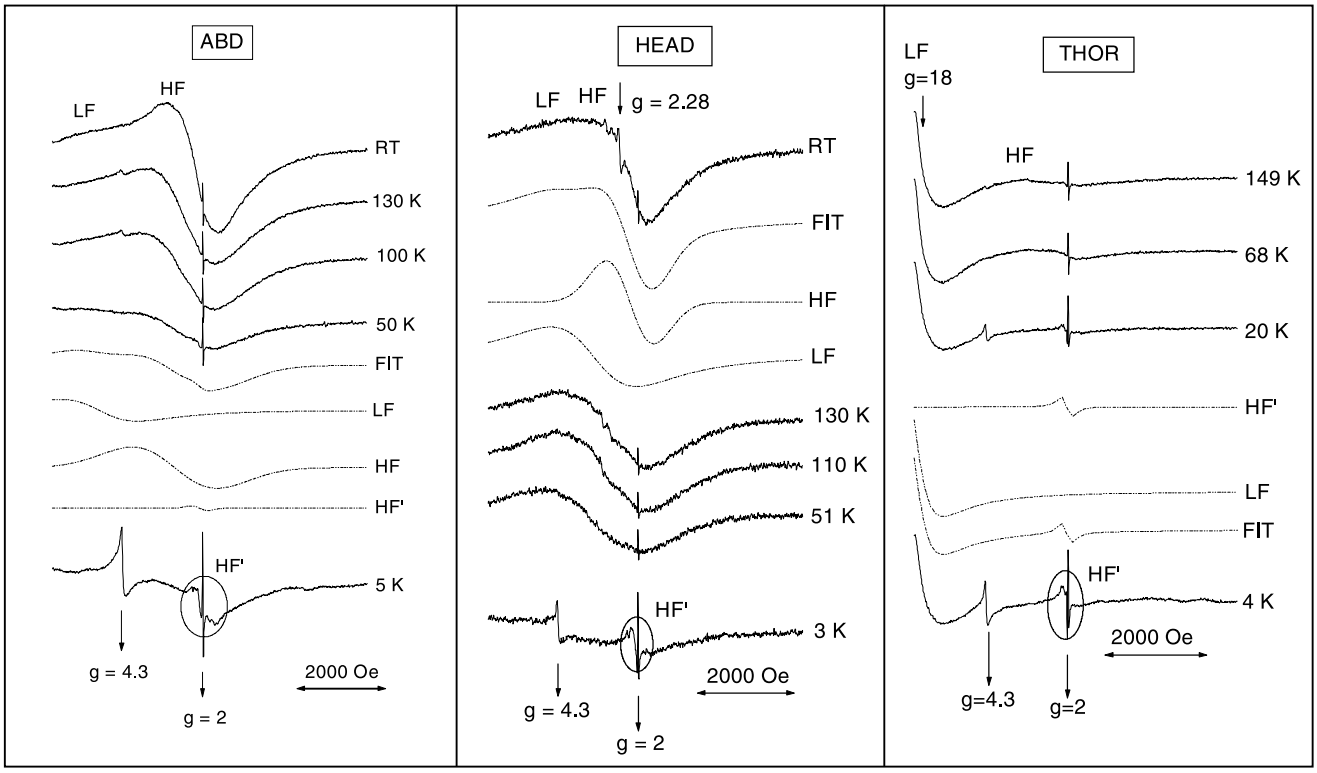

Fig. 1. Spectra temperature dependence from 3 K to room temperature of head with antennae (HEAD), abdomen with petiole (ABD), and thorax with feet (THOR) of *S. substituta* ants. Dashed lines are the fitted spectra and components of the ABD at 50 K, HEAD at RT, and THOR at 4 K.

estimated at RT for this line and for the HF component, dominant in the HEAD and ABD spectra, yields 8.9×10^9 and 6.4×10^9 a.u. values, respectively. These S ratios show up to nine times more magnetic material amount in the HEAD than in the THOR and 1.4 more than in the ABD. The S ratio between the HEAD (2.5×10^8 a.u.) and ABD (1.8×10^8 a.u.) are confirmed by calculating the double integration of the FMR spectra, taken at the sample position of maximum signal intensity.

The fitting procedure leads to the H_R and ΔH_{pp} temperature dependences of the HF and LF components (Fig. 2). The HF′ parameters are temperature independent within the experimental error bars (not shown). From H_R values the demagnetization field, H_D, and the anisotropy field, H_A, are estimated under the considerations described below, that are based on the parallel behavior of the LF and HF H_R curves, as previously used [14,15]

$$\hbar\omega_0 = g\beta H_{ef} = g\beta(H_R + H_D + H_A). \quad (2)$$

H_R is the external field value where the spectra derivative intensity is null, then

$$H_R = \hbar(\omega_0/g\beta) - (N_\perp - N_{//})M_S - H_A, \quad (3)$$

where $N_\perp$ and $N_{//}$ are the perpendicular and parallel demagnetizing tensor components and M_S is the saturation magnetization.

Isolated spherical nanoparticles are associated to the HF component without H_D contribution. The LF component is related to large particles or clusters, assuming a prolate ellipsoid with the three principal geometrical axes (a, b, and c) satisfying $c \gg a = b$ and $q = c/b$. The demagnetizing tensor components are given by [14,28]

$$N_{//} = N_c = 4\pi\{q\ln[q + (q^2-1)^{1/2}]/(q^2-1)^{1/2} - 1\}/(q^2-1) \quad (4)$$

with $N_{//} + 2N_\perp = 4\pi$.

H_D is then calculated by the difference between the LF and HF values of H_R in the temperature range where the curves are parallel. H_D are estimated as 1510 ± 170 Oe for ABD, 1913 ± 148 Oe for HEAD, and 3190 ± 93 Oe for THOR in the temperature ranges 5–177 K, 3–90 K, and 90–297 K, respectively. Taking the magnetite saturation magnetization as 470 G, the calculated H_D match $q = 2$ and 3, suggesting a linear chain of two and three nanoparticles for ABD and HEAD, respectively, while, for THOR $q > 300$, suggesting a bulk-like magnetite structure. Similar results are obtained if maghemite ($M_S = 420$ G) is considered.

The extrapolated g values from the high temperature region in Fig. 2 are $g = 2.05 \pm 0.01$ for ABD, 2.11 ± 0.01 for HEAD, and 2.14 ± 0.01 for THOR, which are used in Eq. (3), for calculating H_A values (Fig. 3). H_A values obtained from the HF and LF lines

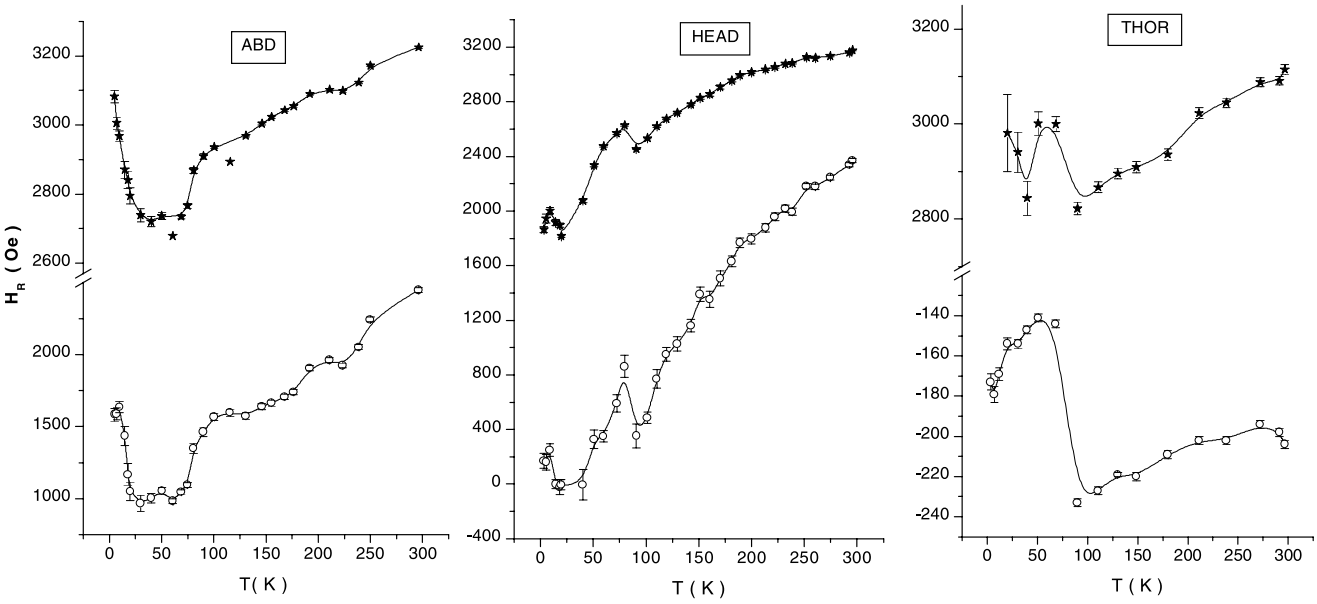

Fig. 2. Temperature dependence of ABD, HEAD, and THOR resonance field: °LF line, *HF line. Solid lines are guides to the eyes.

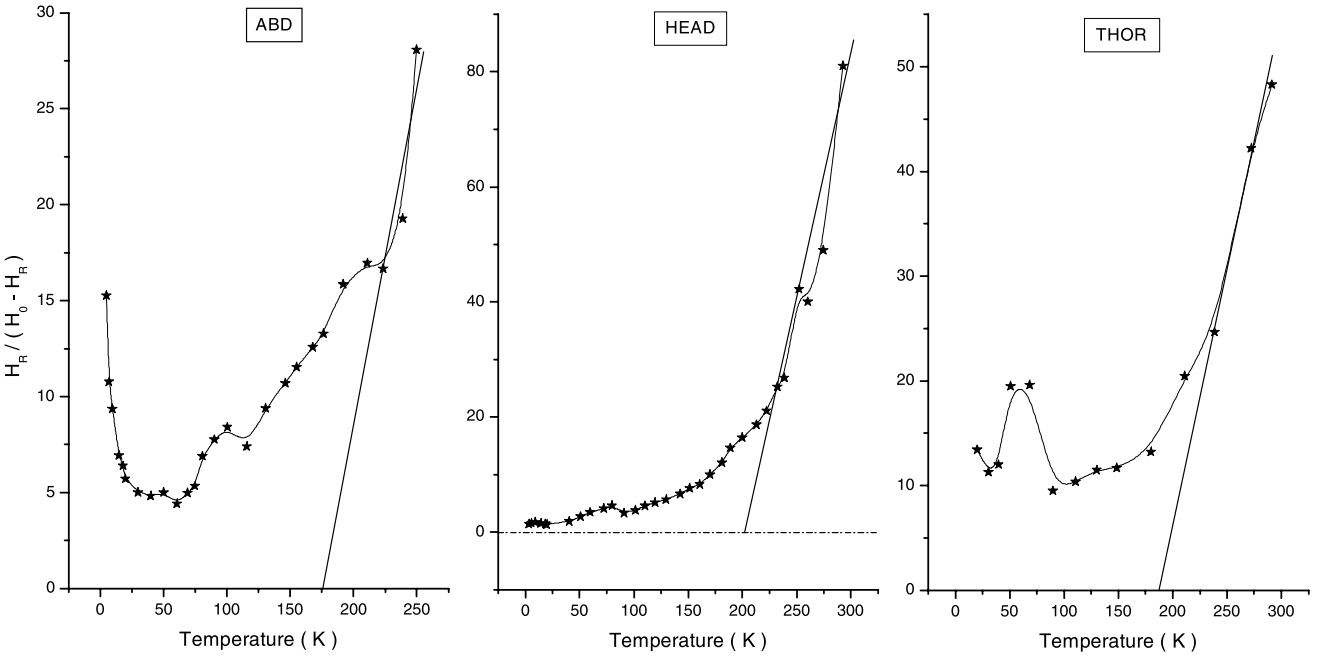

Fig. 3. $H_R/(H_0 - H_R) \propto \chi$ temperature dependence; H_R values of the ABD, HEAD, and THOR HF lines. Solid lines are guides to the eyes.

of ABD and HEAD spectra increase as temperature decreases and both present a temperature transition, T_t, where a H_A decrease is observed. T_t is 108 ± 8 and 122 ± 8 K for the ABD HF and LF lines, respectively, and 85 ± 5 K for both HEAD lines.

The magneto-orientation (T_{or}) or Verwey temperature transition, where H_A is null, are only observed for the LF components (Fig. 3) as 180 ± 10 K for ABD and 145 ± 5 K for HEAD. For the THOR, the T_t and T_{or} temperatures are not determined because of the experimental error bars magnitude.

H_R is also related to χ_m, the magnetic susceptibility of the amorphous boundary region, surrounding superparamagnetic magnetite clusters [29] as

$$\chi_m^{-1} = \lambda H_R(T)/[H_0 - H_R(T)], \quad (5)$$

where λ is the interaction constant and H_0 is the high temperature saturation value of H_R. H_0 was extrapolated from Fig. 2 as 3285 ± 31, 3200 ± 15, and 3155 ± 16 Oe for ABD, HEAD, and THOR HF lines, respectively. The linear temperature dependence at high temperatures in the plot of $H_R(T)/[H_0 - H_R(T)]$

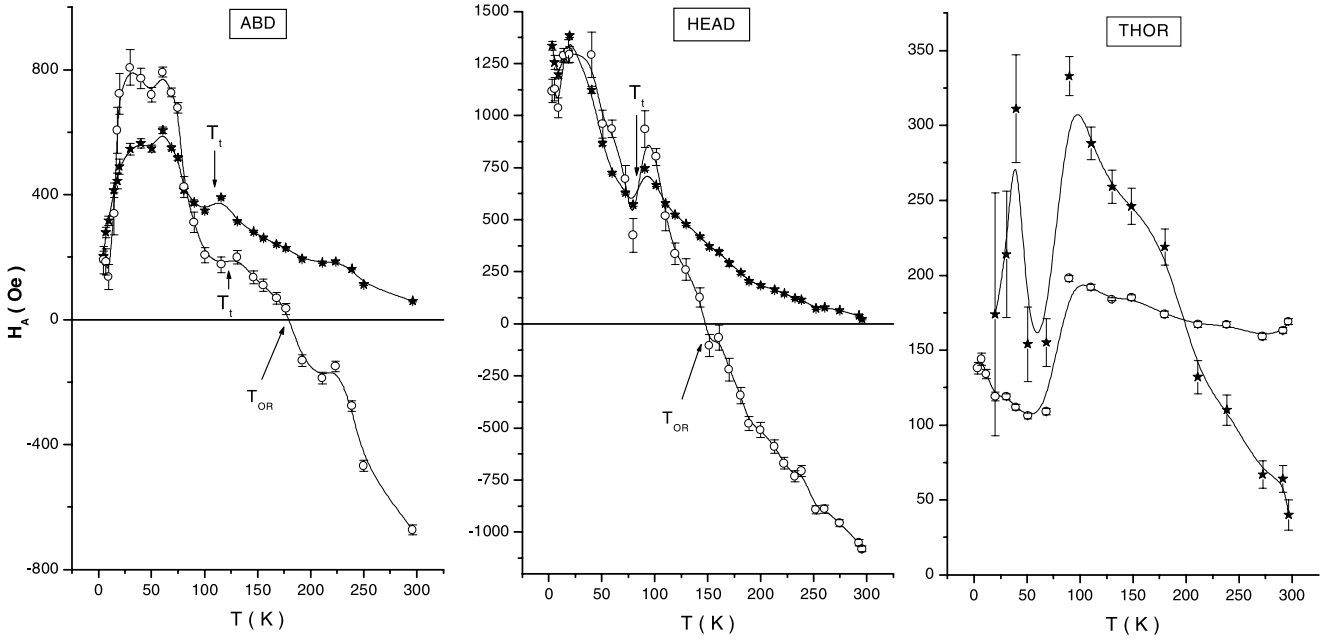

Fig. 4. Anisotropy field temperature dependence of ABD, HEAD, and THOR components: °LF line, *HF line. Solid lines are guide to the eyes.

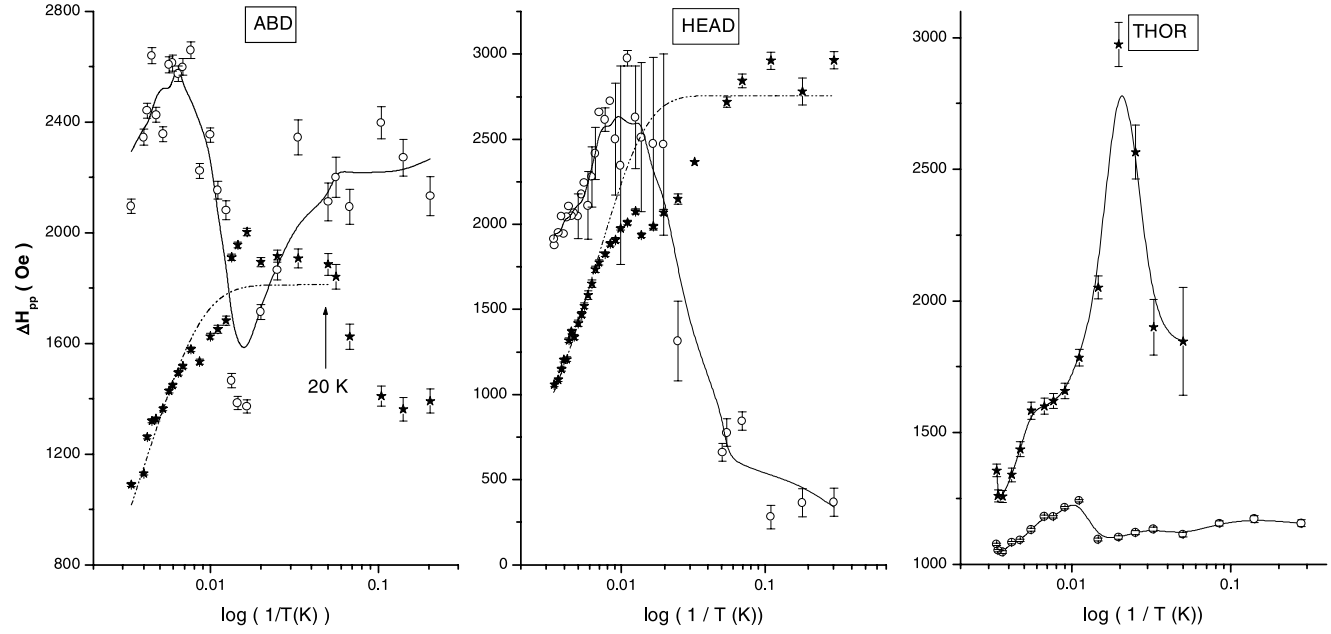

Fig. 5. Linewidth temperature dependence of ABD, HEAD, and THOR components: °LF line, *HF line. Solid lines are guide to the eyes and dashed lines are the fitted curves.

confirms a Curie–Weiss temperature for the cluster (Fig. 4). Since LF components are associated to aggregate or large particles, these temperatures are determined only for the HF lines of HEAD, ABD, and THOR isolated nanoparticles as 175 ± 15 K, 200 ± 20 K, and 190 ± 20 K, respectively.

The temperature dependences of the HF and LF linewidths of HEAD, ABD, and THOR spectra are given in Fig. 5. The solid lines are guide to the eyes. Based on the assumption of isolated spherical nanoparticles, the HF linewidths temperature dependence are fitted using the equation

$$\Delta H_{\mathrm{pp}} = \Delta H^0 \tanh(\Delta E/2k_{\mathrm{B}}T),$$

where ΔH^0 is the low temperature limit value, ΔE the magnetic energy KV, V is the nanoparticle magnetic volume,

and k_B the Boltzman constant. The dashed lines in Fig. 5 are the best fitting curves with $\Delta H^0 = 1866 \pm 32$ and 2457 ± 50 Oe and $\Delta E/2k_B = 177 \pm 9$ and 114 ± 4 K for ABD ($T > 20$ K) and HEAD, respectively. As K is temperature-dependent, ΔE is taken as $K_{ef} V$ with $K_{ef} = M_s\langle - H_A\rangle/2$, where $\langle H_A\rangle$ is the mean value obtained from Fig. 3 data (203 Oe for ABD and 216 Oe for HEAD) for temperatures above T_t. Magnetic volumes are estimated in $(1.0 \pm 0.1) \times 10^3$ nm^3 and $(6.2 \pm 0.2) \times 10^3$ nm^3 and correspond to mean particle diameters of 12.5 ± 0.1 and 11.0 ± 0.2 nm in ABD and HEAD.

4. Discussion

The FMR results presented provide evidence of magnetic material in the three body parts of *Solenopsis* ants. The differences among the spectra parts evidence that the cleaning procedure was successful in eliminating magnetic particles trapped on the ant fur, however, ingested particles cannot be discarded.

The magnetic material (ferro(i)magnetic, superparamagnetic, and paramagnetic) contributing to the FMR spectra is not uniformly distributed in the ant body parts. From the S estimates, at least 45% of the magnetic material is in the *S. substituta* body (thorax plus abdomen). For comparison, only 34% of the ferrimagnetic saturation magnetization comes from the body of *P. marginata* ant [22]. RT saturation magnetization values of the migratory ant show the head plus antennae with the highest magnetic contents, with ratios of 4.3 and 3.5 relative to the abdomen and thorax [22] to be compared to 1.4 and up to 9, respectively, in *S. substituta*.

The two ferrimagnetic broad lines (HF, LF) observed in the spectra of *S. substituta* HEAD and ABD were previously observed in migratory ant [14] and honeybee [15] smashed abdomens indicating the presence of similar magnetic materials. The LF thorax line was related to large particles as those of natural mineral magnetite [30] as observed for whole bodies of another *Solenopsis* species [4]. The HF′ component observed in the spectra of the three body parts has been associated to FeOOH [31], considered as the precursor of biogenic magnetite in bacteria, nematodes, and bees [32,33,15].

For temperatures above 90 K, the LF and HF components of the three body parts are shifted to low fields as temperature decreases, a typical behavior observed for synthetic oxide nanoparticles [30] as well as for those found in insects [14,15,24], in particular, magnetite and maghemite as reported for nanoparticles in migratory ant abdomens [3]. The estimated Curie–Weiss temperatures of the particles in the three body parts are in good agreement with 180 K obtained for 40–55 Å superparamagnetic magnetite cluster sizes [29], as well as the g values extrapolated for high temperatures with the magnetite one, 2.12 [34,35]. These results support the hypothesis of magnetite as the magnetic particle constituent in the *Solenopsis* ant parts.

The properties of magnetite in the low-temperature transition region from 100 to 135 K are still unclear. The transition temperature, T_t, associated to electronic properties in the 100–120 K range and the ordering temperature, T_{or}, related to magneto-orientation in the 130–135 K range, where the anisotropy is zero [36], were proposed [37]. The ABD and HEAD presented a T_t lower than the T_{or} as proposed by Belov [37]. T_{or} could only be estimated for the LF components of ABD and HEAD and the values were shifted to high temperatures compared to those in [37]. Nevertheless, the Verwey temperature is sensitive to several factors as the presence of impurities [38] and oxidation degree. Oxidation can suppress the transition and it affects more intensively small grains. This fact can explain the transition disappearance for nanoparticles associated to the HF component that are smaller than those related to the LF one [39]. The T_{or} estimates strongly depend on the g values, which were extrapolated from the experimental data. Taking the bulk magnetite, $g = 2.12$, T_{or} are shifted to lower temperatures (88 ± 5 and 130 ± 3 K for the ABD LF and HF; 130 ± 5 and 181 ± 3 K for HEAD LF and HF, respectively).

The highest magnetic material content was found in the head with antennae, certainly biomineralized while ingested particles in the ABD and THOR cannot be discarded. A controlled diet would be necessary [40] to

Table 1
FMR magnetic parameters of isolated nanoparticles in social insects

Social insect	Body part	KV (10^{-14} erg)	K_{ef} (10^4 erg/cm^3)	Magnetic volume (10^3 nm^3)	Reference
S. substituta[a]	Head	3.1	5.1	0.62	This paper
	Abdomen	4.9	4.8	1.0	This paper
P. marginata[a]	Abdomen	7.5	6.4 ± 04	1.2	[14]
A. mellifera[a]	Abdomen	2	1.9	1.0	[15]
N. opacus[b]	Head	6.7	2.1 ± 0.1	3.2	[24]
	Abdomen + thorax[c]	8.8	2.6 ± 0.1	3.4	

[a] Smashed.
[b] Intact body part.
[c] Oriented.

eliminate these particles, but this was not possible in this study with ants collected in natural habitat. Although the magnetic material found in the three body parts can be connected to the nervous system cells, this result is not sufficient to conclude about their role in the magnetoreception mechanism.

Table 1 summarizes FMR parameters of isolated nanoparticles of some social insects, although sample preparations vary among them. From the volumes in this table, diameters of 11.0 ± 0.2 and 12.5 ± 0.1 nm, for *S. substituta* HEAD and ABD were obtained in the same superparamagnetic region of those found in *P. marginata*ants (13.0 ± 0.4 nm) and in *N. opacus* termites (18.5 ± 0.3 nm) using FMR [14,24]. The magnetic volume of the abdomen nanoparticles of the two ants and bee are very similar. On the other hand, the magnetic anisotropy constant and magnetic volumes are different in different body parts of the *S. substituta* ant while such a difference is not observed for the termite particles. The magnetic size and property diversity shown in Table 1 stimulates a comparison among social insects. A wide set of magnetic data for different species can help to distinguish general and specific material properties related to magnetoreception models. This paper points to the possibility of systematizing the study of magnetic material, in particular by FMR. For a more detailed analysis, FMR results must be considered together with other magnetic techniques as well as electron microscopy, having as the final goal correlating magnetic material properties to their physiological function.

Acknowledgments

We are thankful to Dr. Ana Y. Harada Entomological Collection Curator of the Emilio Goeldi Paraense Museum, Zoology Department for specie classification, Dr M.H. Prado da Silva for carefully reading the paper and we thank CNPq and FAPERJ for financial support.

References

[1] M. Vácha, Magnetic orientation in insects, Biologia 52 (1997) 629–636.
[2] R. Wiltschko, W. Wiltschko, Magnetic Orientation in Animals, Springer, Berlin, 1995.
[3] D. Acosta-Avalos, E. Wajnberg, P.S. Oliveira, I. Leal, M. Farina, D.M.S. Esquivel, Isolation of magnetic nanoparticles from *Pachycondyla marginata* ants, J. Exp. Biol. 202 (1999) 2687–2692.
[4] D.M.S. Esquivel, D. Acosta-Avalos, L.J. El-Jaick, A.D.M. Cunha, M.G. Malheiros, E. Wajnberg, M.P. Linhares, Evidence for magnetic material in the fire ant *Solenopsis* sp. by electron paramagnetic resonance measurements, Naturwissenschaften 86 (1999) 30–32.
[5] J.L. Kirschvink, A.K. Kirschvink, B.J. Woodford, Magnetite biomineralization in the human brain, Proc. Natl. Acad. Sci. USA 26 (1992) 7683–7687.
[6] J. Dobson, Investigation of age-related variations in biogenic magnetite levels in the human hippocampus, J. Exp. Brain Res. 144 (2000) 122–126.
[7] A.F. Davila, G. Fleissner, M. Winklhofer, N. Petersen, A new model for a magnetoreceptor in homing pigeons based on interacting clusters of superparamagnetic magnetite, Phys. Chem. Earth 28 (2003) 647–652.
[8] M. Hanzlik, C. Heunemann, E. Holtkamp-Rötzler, M. Winklhofer, N. Petersen, G. Fleissner, Superparamagnetic magnetite in the upper-beak tissue of homing pigeons, Biometals 13 (2000) 325–331.
[9] Y. Çamlitepe, D.J. Stradling, Wood ants orient to magnetic fields, Proc. R. Soc. Lond. B 261 (1995) 37–41.
[10] R. Gander, U. Gander, The light and magnetic compass of the weaver ant, *Oecophylla smaragdina* (Hymenoptera: Formicidae), Ethology 104 (1998) 743–758.
[11] A.N. Banks, R.B. Srygley, Orientation by magnetic field in leafcutter ants, *Atta colombica* (Hymenoptera: Formicidae), Ethology 109 (2003) 835–846.
[12] J.B. Anderson, R.K. Vander Meer, Magnetic orientation in fire ant, *Solenopsis invicta*, Naturwissenschaften 80 (1993) 568–570.
[13] J.H. Klotz, L.L. Van Zandt, B.L. Reid, G.W. Bennett, Evidence lacking for magnetic compass orientation in fire ants (Hymenopotera: formicidae), J. Kansas Entomol. Soc. 70 (1) (1997) 64–65.
[14] E. Wajnberg, D. Acosta-Avalos, L.J. El-Jaick, L.G. Abraçado, J.L.A. Coelho, A.F. Bakusis, P.C. Morais, D.M.S. Esquivel, Electron paramagnetic resonance study of the migratory ant *Pachycondyla marginata* abdomens, Biophys. J. 78 (2000) 1018–1023.
[15] L.J. El-Jaick, D. Acosta-Avalos, D.M S. Esquivel, E. Wajnberg, M.P. Linhares, Electron paramagnetic resonance study of honeybee *Apis mellifera* abdomens, Eur. Biophys. J. 29 (2001) 579–586.
[16] B.P. Weiss, S.S. Kim, J.L. Kirschvink, R.E. Kopp, M. Sankaran, A. Kobayashi, A. Komeili, Ferromagnetic resonance and low-temperature magnetic tests for biogenic magnetite, Earth Planet. Sci. Lett. 224 (2004) 73–89.
[17] J.L. Gould, J.L. Kirschvink, K.S. Deffeyes, Bees have magnetic remanence, Science 210 (1978) 1026–1028.
[18] J.L. Kirschvink, Magnetite biomineralization and geomagnetic sensitivity in higher animals: an update and recommendations for future study, Bioeletromagnetics 10 (1989) 239–259.
[19] J.L. Gould, J.L. Kirschvink, K.S. Deffeyes, M.L. Brines, Orientation of demagnetized bees, J. Exp. Biol. 80 (1980) 1–8.
[20] M.M. Walker, M.E. Bitterman, Short communication attached magnets impair magnetic field discrimination by honeybees, J. Exp. Biol. 141 (1989) 447–451.
[21] S. Takagi, Paramagnetism in honeybees, J. Phys. Soc. Jpn. 64 (1995) 4378–4382.
[22] E. Wajnberg, G. Cernicchiaro, D.M.S. Esquivel, Antennae: the strongest magnetic part of the migratory ant, BioMetals 168 (2004) 246–251.
[23] D. Acosta-Avalos, D.M.S. Esquivel, E. Wajnberg, H.G.P. Lins e Barros, P.S. Oliveira, I. Leal, Seasonal patterns in the orientation system of the migratory ant *Pachycondyla marginata*, Naturwissenschaften 88 (2001) 343–346.
[24] O.C. Alves, E. Wajnberg, J.F. de Oliveira, D.M.S. Esquivel, Magnetic material arrangement in oriented termites: a magnetic resonance study, J. Magn. Res. 168 (2004) 246–251.
[25] B.A. Maher, Magnetite biomineralization in termites, Proc. R. Soc. Lond. B 265 (1397) (1998) 733–737.
[26] E.M. Yahiaoui, R. Berger, Y. Servant, J. Kliava, L. Cugunov, A. Mednis, Electron paramagnetic resonance of Fe^{3+} ions in borate glass computer simulation, J. Phys. Condens. Matter 6 (1994) 9415–9428.

[27] P.F. Knowles, D. Marsh, H.W.E. Rattle, Magnetic Resonance of Biomolecules, Wiley, London, 1976.
[28] S.V. Vonsovskii, Ferromagnetic Resonance, Pergamon Press, New York, 1966.
[29] M. Hagiwara, K. Nagata, Magnetic behaviors of complex nature found in an oxide glass system containing deposited magnetite clusters at the superparamagnetic state, J. Magn. Magn. Mater. 177–181 (1998) 91–92.
[30] M. Ikeya, Silica and silicates: geotherm and volcanism, in: M.R. Zimmerman, N. Whitehead (Eds.), New Applications of Electron Spin Resonance Dating, Dosimetry and Microscopy, World Scientific, London, 1993.
[31] A. Boughriet, C. Codier, L. Derane, B. Ouddane, H. Chamley, M. Warlel, Coprecipitation/accumulation/distribution of manganese and iron, and electrochemical characteristics of Mn in calcareous seawater, Fresenius, J. Anal. Chem. 352 (1995) 341–353.
[32] S. Mann, N.H.C. Sparks, V.J. Wade, in: R.B. Frankel, R.P. Blakemore (Eds.), Iron Biominerals, Plenum Press, New York, 1991.
[33] C.G. Cranfield, A. Dawe, V. Karloukovski, R.E. Dunin-Borkowski, D. Pomerai, J. Dobson, Biogenic magnetite in the nematode *Caenorhabditis elegans*, Proc. R. Soc. Lond. Ser. B 271 (57) (2004) S436–S439.
[34] Z. Kakol, J.M. Honig, Influence of deviations from ideal stoichiometry on the anisotropy parameters of magnetite $Fe_{3(1-\delta)}O_4$, Phys. Rev. B 40 (1989) 9090–9097.
[35] K. Abe, Y. Mijamoto, S. Chikazumi, Magnetocrystalline anisotropy of low-temperature phase of magnetite, J. Phys. Soc. Jpn. 41 (1976) 1894–1902.
[36] J. García, G. Subías, The Verwey transition-a new perspective, J. Phys. Condens. Matter 16 (2004) R145–R178.
[37] K.P. Belov, Electronic processes in magnetite (or 'enigmas of magnetite'), Phys. Usp. 36 (1993) 380–391.
[38] N. Guigue-Millot, N. Keller, P. Perriat, Evidence for the Verwey transition in highly nonstoichiometric nanometric Fe-based ferrites, Phys. Rev. B 64 (1) (2001). Art. No. 012402.
[39] O. Ozdemir, D.J. Dunlop, B.M. Moskowitz, The effect of oxidation on the Verwey transition in magnetite, Geophys. Res. Lett. 20 (1993) 1671–1674.
[40] J.F. Oliveira, E. Wajnberg, D.M.S. Esquivel, O.C. Alves, Magnetic resonance as a technique to magnetic biosensors characterization in *Neocapritermes opacus* termites, J. Magn. Magn. Mater. doi:10.1016/j.jmmm.2005.03.078.